ACS APPLIED NANO MATERIALS

www.acsanm.org Article

Carbon-Doping Mesoporous β-Mo_2C Aggregates for Nanomolar Electrochemical Detection of Hydrogen Peroxide

Bo Li, Li-Hong Liu, Hai-Yan Song, Zhao-Peng Deng,* Li-Hua Huo, and Shan Gao*

Cite This: *ACS Appl. Nano Mater.* 2020, 3, 7499−7507 Read Online

ACCESS | Metrics & More | Article Recommendations | Supporting Information

ABSTRACT: The development of a nonenzymatic electrochemical sensor with nanomolar detection of H_2O_2 has been highly desirable due to its wide applications in bioanalysis. In this paper, the glassy carbon electrode (GCE) modified by carbon-doping molybdenum carbide (β-Mo_2C/C/GCE) was simply fabricated by simple drop-coating method and used to detect H_2O_2 in pretreated human serum. The β-Mo_2C/C hierarchical structure is obtained by a one-step pyrolysis of the single-crystal $[(H_2L)_2(Mo_8O_{26})]_n$ [L = *N*,*N*′-bis(3-pyridin)-1,4-xylyenediamine] and constructed from amounts of nanoparticles (~10 nm) with a mesoporous size distribution of 42.46 nm. At room temperature, the β-Mo_2C/C/GCE sensor has a high sensitivity of 247.73 μA mM^{-1} cm^{-2}, a low detection limit of 90 nM (signal/noise = 3), as well as a wide linear range of 0.27 μM−2.39 mM, and it shows better electrocatalytic performance of H_2O_2 than the molybdenum oxide (obtained from the same precursor) modified glassy carbon electrode (α-MoO_3/GCE). Such outstanding electrocatalytic performances are related to the synergistic effect of the inherent characteristics of the β-Mo_2C/C material. The satisfactory test results of the human serum samples indicate that the β-Mo_2C/C/GCE sensor can be used as a good candidate for real-time detection of H_2O_2 in biological, food, and environmental fields.

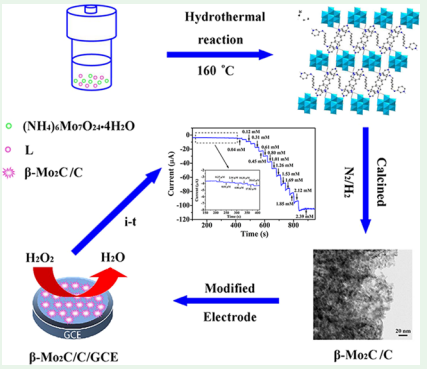

KEYWORDS: *β-Mo_2C, nonenzymatic sensor, H_2O_2, mesoporous structure, pyrolysis*

INTRODUCTION

Hydrogen peroxide (H_2O_2), as a common small molecular compound with oxidation and reduction, is widely used in the fields of pharmacy, clinic, bioanalysis, food, environmental protection, and other chemical industries. As a byproduct of cell metabolism, H_2O_2 plays an important role in different biological systems, such as immune cell activation, cell proliferation, protein synthesis, and plant root growth.[1] The appropriate concentration of H_2O_2 (1−700 nM) is conducive to intracellular information transmission. However, when the concentration of H_2O_2 is more than 700 nM, it is likely to cause cell damage and gene mutation, further inducing diabetes, arteriosclerosis, Alzheimer's disease, cancer, and other diseases.[2−6] Thereby, the detection of H_2O_2 in human serum is beneficial to the early screening of some cancers, vascular diseases, and so on. Thus, developing a fast, precise, and efficient detection method of nanomolar-level H_2O_2 is definitely crucial to disease diagnosis, environmental production, and food safety.

At present, the methods of fluorescence analysis,[7] spectrophotometry,[8] and electrochemical sensors[9] have been applied to the detection of H_2O_2. Among them, the electrochemical sensor has recently attracted considerable attention owing to its advantages of high sensitivity, easy portability, and low detection limit. Especially, compared with the enzyme-based sensor with high price and short life, the research on nonenzymatic H_2O_2 sensor with low cost, high selectivity, convenient operation, and well stability has been fascinating.[10] Although noble metals and their sensitized nanomaterials show good electrocatalytic properties,[11] the commercial application of such sensors is limited due to their scarce resource, high price, and the possibility of Cl^- poisoning. In recent years, the nonenzymatic electrochemical sensors assembled from the hierarchical metal oxides nanostructures with good stability and catalytic properties, such as MnO_2,[12] Co_3O_4,[13] CuO,[14] Fe_3O_4,[15] Mn_2CuO_4,[16] etc., have good application prospects in the field of H_2O_2 detection. However, most of the reported nonenzymatic sensors based on metal oxides have low selectivity and high detection limit (>μM level of H_2O_2), which make them difficult to detect nanomolar-level H_2O_2 in biological analysis such as human serum.[17] In addition, fine synthetic methods in many reported hierarchical micro/nanostructure materials are difficult and complicated and also hinder their practical applications.[18,19] Therefore, it is a great challenge to simply prepare non-

Received: April 24, 2020
Accepted: July 7, 2020
Published: July 7, 2020

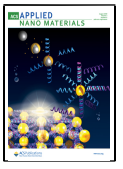

https://dx.doi.org/10.1021/acsanm.0c01106
ACS Appl. Nano Mater. 2020, 3, 7499−7507

Scheme 1. Schematic Representation for the Preparation of β-Mo_2C/C and α-MoO_3 Materials

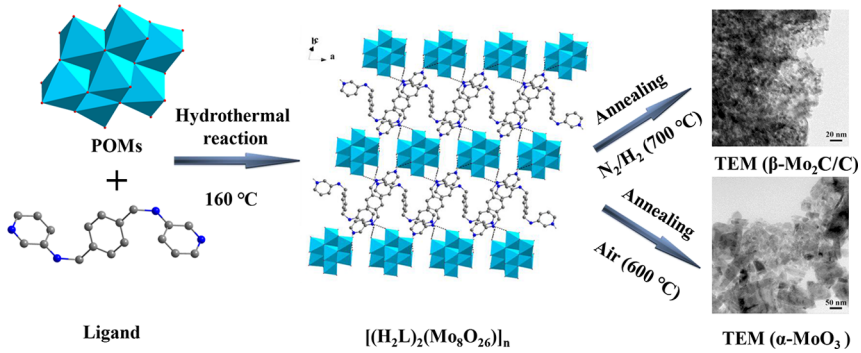

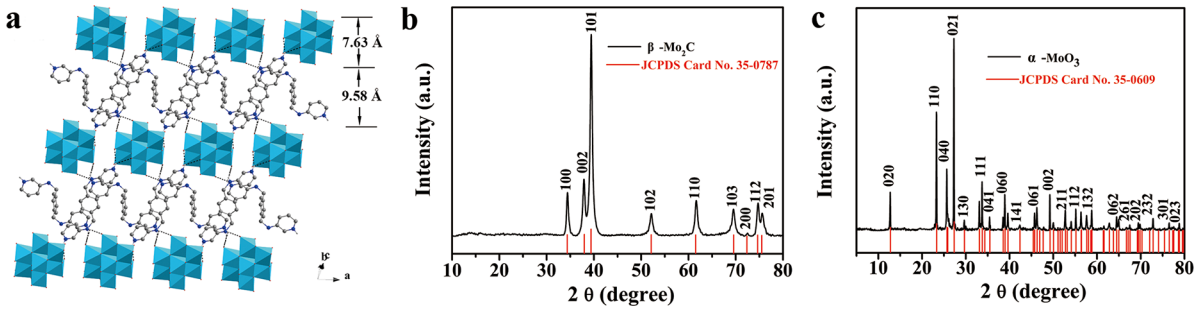

Figure 1. (a) 2-D layered structure of the hybrid $[(H_2L)_2(Mo_8O_{26})]_n$ compound; XRD patterns of β-Mo_2C/C (b) and α-MoO_3 (c) samples.

enzymatic electrochemical H_2O_2 sensors with high selectivity and low nanomolar-level detection limit.

Molybdenum carbide has recently attracted great interests due to its high conductivity, good stability, and catalytic property, and it has potential applications in solar cells, superconductivity, lithium−sulfur batteries, and the hydrogen evolution reaction.[20,21] Unfortunately, the well-biocompatibility of Mo_2C has been rarely reported in the application of electrochemical sensors as electrode material. In 2016, Zhai et al. fabricated an electrochemical sensor by Mo_2C nanotube/thionin, which exhibited a detection limit as low as 3 pg mL^{-1} for α-fetoprotein.[22] In the same year, another electrochemical sensor based on a Mo_2C/multiwalled carbon nanotube (MWCNT) with the detection limit of rifampicin (0.045 μM) was also reported.[23] Two years later, a Mo_2C/*n*-carboxymethyl chitosan sensor containing a DNA chain replacement reaction was assembled, which showed the low detection limit of 0.34 fM to RNA-21.[24] Meanwhile, a porous Mo_xC@C nanosphere electrode could detect both guanine and adenine, corresponding to the detection limit of 8.5 and 8.0 nM, respectively.[25] Just recently, an electrochemical sensor constructed from hollow Mo_2C/C spheres was used to determine the presence of hydroquinone, catechol, and resorcinol with the detection limit of 0.12, 0.19, and 1.1 μM, respectively.[26] However, as far as we know, there has been no report of H_2O_2 electrochemical sensor based on molybdenum carbide. Presently, the synthetic methods of molybdenum carbide materials, such as nanoparticles,[27] nanoribbons,[28] two-dimensional (2-D) layer,[29] and porous octahedron,[30] are complicated, time-consuming, and difficult to be produced in practice. In recent years, a simple pyrolysis method using metal−organic frameworks (MOFs) as precursors has been used to prepare metal oxide functional materials with a hierarchical structure.[31] We previously fabricated an α-MoO_3/GO/GCE sensor (GO = graphene oxide; GCE = glassy carbon electrode), which exhibited a good electrocatalytic H_2O_2 property.[32] However, this sensor showed a higher detection limit of 0.31 μM. In view of the good biocompatibility and the electrocatalysis of molybdenum carbide, we tried to prepare Mo_2C by calcining organic−inorganic hybrid $[(H_2L')_2(Mo_8O_{26})]_n$ [HL′ = *N*-(pyridin-3-ylmethyl)pyridine-3-amine] crystal under inert gas atmosphere. Unfortunately, the attempt failed. The reason was probably originated from the infinite one-dimensional (1D) $[(\beta\text{-}Mo_8O_{26})^{4-}]_n$ chain and the small amount of carbon in ligand HL′. Therefore, we designed and synthesized herein a new hybrid supramolecular compound $[(H_2L)_2(Mo_8O_{26})]_n$, in which the ligand (L = *N*,*N*′-bis(3-pyridin)-1,4-xylyenediamine) contains a carbon-rich spacer of the -NH−CH-C_6H_4−CH-NH- group, and the discrete $(\beta\text{-}Mo_8O_{26})^{4-}$ clusters are surrounded by H_2L^{2+} cations. Bearing this conception in mind, in this paper, mesoporous β-Mo_2C/C and α-MoO_3 hierarchical structures were successfully prepared by a one-step pyrolysis in different atmospheres. A novel nonenzymatic electrochemical sensor fabricated from β-Mo_2C/C/GCE was simply fabricated by a simple drop-coating method, which presented excellent electrocatalytic properties to H_2O_2 for the first time. The sensor has a high sensitivity of 247.73 μA mM^{-1} cm^{-2} with a low detection limit of 90 nM (signal/noise (S/N) = 3), and it can be applied to detecting hydrogen peroxide in human serum.

EXPERIMENTAL SECTION

The parts of chemical reagents, characterization instruments, and the synthesis of $[(H_2L)_2(Mo_8O_{26})]_n$ single crystal were listed in the Supporting Information.

Preparation of Mesoporous β-Mo_2C/C and MoO_3 Hierarchical Structures. Scheme 1 presents the synthetic procedure of the β-Mo_2C/C and MoO_3 materials. According to the result of the thermogravimetric (TG) curve of the $[(H_2L)_2(Mo_8O_{26})]_n$ single crystal in a N_2 atmosphere (Figure S3a), molybdenum carbide could be prepared by calcining $[(H_2L)_2(Mo_8O_{26})]_n$ crystals at 700 °C in a

https://dx.doi.org/10.1021/acsanm.0c01106
ACS Appl. Nano Mater. 2020, 3, 7499−7507

reductive circumstance. The porcelain boat loaded with a pure crystal sample was placed in a tubular furnace and then annealed at 700 °C for 2 h in N_2/H_2 atmosphere (nitrogen/hydrogen ratio = 95/5%). Subsequently, the calcined product was separately cleaned with deionized water and ethanol after it cooled to room temperature. Finally, the black β-Mo_2C/C product was obtained and preserved in a desiccator. In addition, according to the TG curve of the $[(H_2L)_2(Mo_8O_{26})]_n$ crystals in an air atmosphere (Figure S3b), a pale blue α-MoO_3 material was synthesized by annealing the crystal sample at 600 °C for 2 h in an air atmosphere.

Fabrication and Electrochemical Measurements of Modified Electrodes. The β-Mo_2C/C/GCE modified electrode was prepared by drop-casting a pretreated 2 mg β-Mo_2C/C sample onto the surface of a cleaned GCE (see the Supporting Information). For comparison, the α-MoO_3 sample was also used to fabricate another modified electrode according to the above similar way, which was named as α-MoO_3/GCE. The electrochemical measurements of these modified electrodes were listed in the Supporting Information.

RESULTS AND DISCUSSION

Structure of $[(H_2L)_2(Mo_8O_{26})]_n$. The supramolecular structure of the compound is composed of one $(\beta$-$Mo_8O_{26})^{4-}$ cluster anion and two protonated H_2L^{2+} organic cations (Figure S1a). Adjacent $(\beta$-$Mo_8O_{26})^{4-}$ cluster anions interact with H_2L^{2+} organic cations through N−H···O interactions to generate an orderly hybrid inorganic−organic layer (Figure 1a). The thickness of the discrete $(\beta$-$Mo_8O_{26})^{4-}$ cluster anion is 7.63 Å, and the distance between adjacent $(\beta$-$Mo_8O_{26})^{4-}$ clusters is 9.58 Å along the *b*-axis. Furthermore, the experimental powder X-ray diffraction (PXRD) pattern is consistent with the data simulated from the single-crystal diffraction, indicating that the single-crystal structure can represent the bulk of the compound (Figure S1b). As we forecasted, the separation of $(\beta$-$Mo_8O_{26})^{4-}$ clusters by H_2L^{2+} organic cations with a carbon-rich spacer of the -NH−CH-C_6H_4−CH-NH- group easily generates the molybdenum carbide material. Therefore, mesoporous β-Mo_2C and α-MoO_3 hierarchical structures could be simply prepared by a one-step calcination of this compound under different atmospheres via the effect of the gas spillover.

Characterization of Mesoporous β-Mo_2C/C and α-MoO_3 Materials. The X-ray diffraction (XRD) patterns of the products obtained from the calcination of the hybrid $[(H_2L)_2(Mo_8O_{26})]_n$ compound in different atmospheres are illustrated in Figure 1b,c. It can be seen that the diffraction peaks of the product sintered in N_2/H_2 correspond well to hexagonal β-Mo_2C (JCPDS No. 35-0787, $P6_3mc$, a = 3.012 Å, b = 3.012 Å, c = 4.735 Å). The diffraction peaks of the product calcined in air are consistent with pure orthorhombic α-MoO_3 (JCPDS No. 35-0609, *Pbnm*, a = 3.963 Å, b = 13.856 Å, c = 3.697 Å), which is evidently different from that in previously reported work (α-MoO_3, JCPDS No. 05-0508).[32] All these strong and sharp peaks indicate that the two products have good crystallinization, and no diffraction peaks of other Mo compounds are observed. To further explore element compositions and valence states, we performed the X-ray photoelectron spectroscopy (XPS) analysis of a β-Mo_2C sample. The full survey of the XPS spectrum (Figure S4a) indicates that the calcined product in a N_2/H_2 atmosphere contains Mo, C, and O elements without other impurities, corresponding to the result of energy-dispersive X-ray spectroscopy (EDS) analysis (Figure S4b). It should be indicated that the existence of a small amount of the O element originates from the oxidization of surface trace Mo_2C to MoO_x during the testing process, and the annealed product contains ∼21 wt % carbon besides β-Mo_2C. Thereby, the calcined product in the N_2/H_2 atmosphere can be identified as β-Mo_2C/C composite.

The deconvoluted Mo 3d XPS spectrum is displayed in Figure 2a. The two fitted peaks at 228.6 and 231.6 eV can be

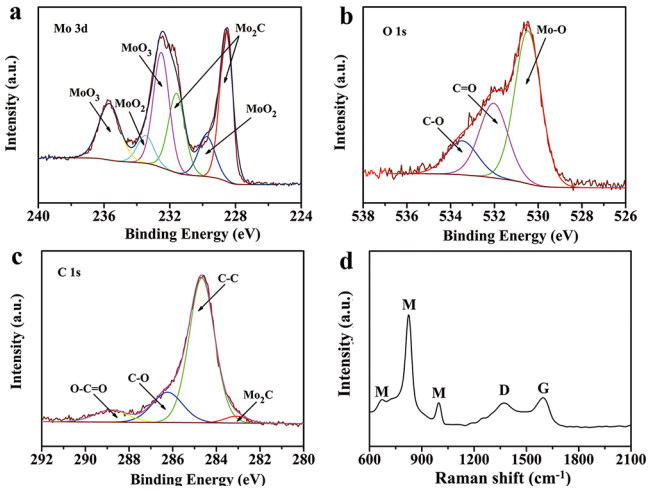

Figure 2. HR XPS spectra of Mo 3d (a), O 1s (b), and C 1s (c) and a Raman spectrum (d) of β-Mo_2C/C sample.

assigned to Mo $3d_{5/2}$ and Mo $3d_{3/2}$ in Mo_2C.[33] The two peaks located at 229.8 and 233.5 eV can be recognized as Mo $3d_{5/2}$ and Mo $3d_{3/2}$ in MoO_2, while the two binding energies of 232.5 and 235.7 eV can be identified as Mo $3d_{5/2}$ and Mo $3d_{3/2}$ in MoO_3, further indicating the existence of the Mo^{4+} and Mo^{6+} valences in final product.[34] These results indicate that a small amount of unsaturated Mo_2C on the surface of the material transfers into MoO_2 and MoO_3 during the XPS measurement. In the high-resolution (HR) O 1s XPS spectrum (Figure 2b), three peaks at 530.5, 532.0, and 533.5 eV correspond to Mo−O, C═O, and C−O.[35] From the HR C 1s XPS spectrum (Figure 2c), the peak located at 283.1 eV can be ascribed to the Mo−C bond in Mo_2C,[36] while the three deconvoluted peaks with the binding energies at 284.7, 286.2, and 288.8 eV can be ascribed to C−C, C−O, and O−C═O, respectively. To further verify the form of carbon, a Raman spectrum of the Mo_2C/C composite was performed. As illustrated in Figure 2d, the three peaks located at 666, 824, and 996 cm^{-1} belong to the characteristic vibrations of Mo_2C.[37] The characteristic D- and G-bands of the carbon at 1368 and 1597 cm^{-1} can be clearly observed. The D-band is associated with partial disordered structure or structural defect in the carbon matrix, while the G-band is concerned with the degree of graphitization, representing the E_{2g} vibration mode of sp^2-hybridized graphite-like carbon.[38] The intensity ratio of D and G peaks (I_D/I_G) can reveal the degree of disorder and defect in the carbon material. It can be inferred from the I_D/I_G value of 0.91 that the residual carbon in the β-Mo_2C/C sample is mainly the amorphous carbon. In addition, the results of the XPS spectra also demonstrate that the calcined product in an air atmosphere contains Mo and O elements apart from the C 1s peak at 284.6 eV as a reference (Figure S5a). The HR Mo 3d spectrum (Figure S5b) exhibits two characteristic peaks located at 232.5 and 235.7 eV, corresponding to the Mo $3d_{3/2}$ and Mo $3d_{5/2}$ spin−orbit peaks of the α-MoO_3 phase. For the HR O 1s spectrum (Figure S5c), the three fitted peaks at 530.4, 531.9, and 533.1 eV are assigned to lattice oxygen,

https://dx.doi.org/10.1021/acsanm.0c01106
ACS Appl. Nano Mater. 2020, 3, 7499−7507

surface adsorbed oxygen, and hydroxyl oxygen, respectively. Therefore, the PXRD and XPS results demonstrate that the calcined product in an air atmosphere is pure orthorhombic α-MoO_3 phase.

The morphologies of β-Mo_2C/C and α-MoO_3 samples display irregular quasi-microspheres, and some macropores and cracks exist on their rough surface due to the effect of the gas spillover during the pyrolysis of the hybrid $[(H_2L)_2(Mo_8O_{26})]_n$ compound (Figures S6 and S7). The fine structures of the β-Mo_2C/C and α-MoO_3 samples can be observed by transmission electron microscopy (TEM) technology after an ultrasound treatment in an ethanol solution. As shown in Figure 3a, the hierarchical structure of

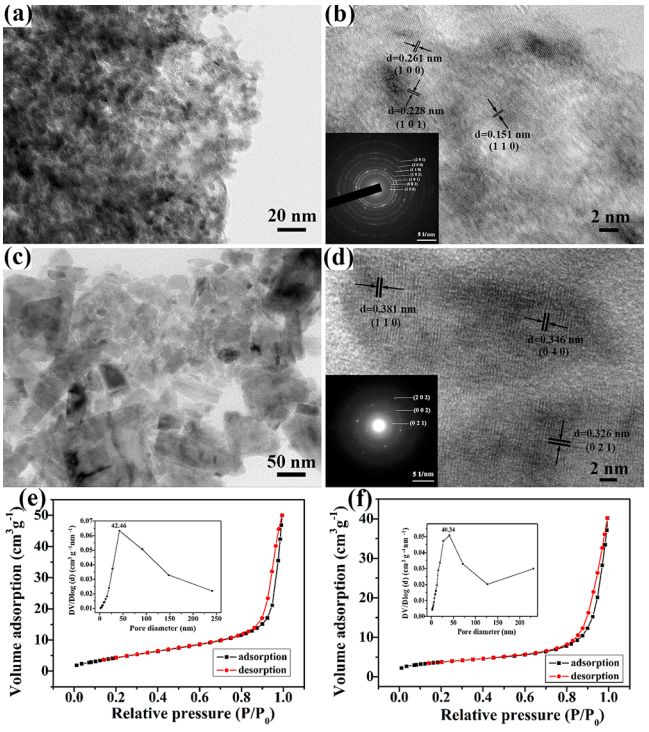

Figure 3. TEM images of the β-Mo_2C/C sample: (a) low magnification; (b) HRTEM and SAED (inset), TEM images of α-MoO_3 sample; (c) low magnification; (d) HRTEM and SAED (inset); N_2 adsorption−desorption isotherms and pore-size distribution (inset) of the β-Mo_2C/C (e) and α-MoO_3 (f) samples.

the β-Mo_2C/C sample is constructed from amounts of ∼10 nm nanoparticles, and there are many mesopores on the surface, which can improve the surface area and electrocatalytic activity of the β-Mo_2C/C material. The HR TEM image (Figure 3b) displays the lattice fringes of 0.261, 0.228, and 0.151 nm, corresponding to the d-values of (100), (101), and (110) crystalline planes of hexagonal β-Mo_2C (JCPDS No. 35-0787). The selected area electron diffraction (SAED) pattern (inset of Figure 3b) exhibits a series of clear diffraction rings, indicating the polycrystalline structure of the β-Mo_2C/C material. In contrast, the TEM image of mesoporous α-MoO_3 shows that the hierarchical structure is constructed from various nanosheets with the size smaller than 100 nm (Figure 3c). The HRTEM image in Figure 3d shows the lattice fringes with a d-spacing of 0.381, 0.346, and 0.326 nm, corresponding to (110), (040), and (021) crystalline planes of orthorhombic α-MoO_3 (JCPDS No. 35-0609). In the corresponding SAED pattern (inset of Figure 3d), the marked diffraction rings with the (021), (002), and (202) crystalline planes indicate that orthorhombic α-MoO_3 has a polycrystalline structure. The nitrogen adsorption−desorption curves of β-Mo_2C/C and α-MoO_3 samples are all assigned the type IV isotherm with an H3 hysteresis loop (P/P_0 > 0.8), demonstrating the existence of the mesoporous structure (Figure 3e,f). The mesoporous sizes are mainly distributed at 42.46 (β-Mo_2C/C) and 40.34 nm (α-MoO_3). Such mesopores are mainly formed by the cross-linking of nanoparticles and the gas overflow of the organic species decomposition, which are beneficial to the rapid diffusion of the analytes and increase the charge transfer speed between electrode and electrolyte, thus further improving the mass transfer efficiency. The Brunauer−Emmett−Teller (BET) surface area of β-Mo_2C/C is 16.63 m^2/g, which is larger than that of α-MoO_3 (13.36 m^2/g). The relatively large specific surface area and mesoporous structure could efficiently expose more active sites and provide a favorable path for electrolyte transportation and penetration. Therefore, compared with the α-MoO_3 material, the mesoporous β-Mo_2C/C material is expected to obviously improve the electrocatalytic performance for the detection of nanomolar-level H_2O_2.

Electrochemical Behaviors of Modified Electrodes. The electrochemical performances of diverse modified GCEs were characterized by cyclic voltammetry (CV) and electrochemical impedance spectroscopy (EIS) in 5.0 mM $[Fe(CN)_6]^{-3/-4}$ (1:1) containing 0.1 M KCl. As illustrated in Figure 4a, the peak current of β-Mo_2C/C/GCE is higher than

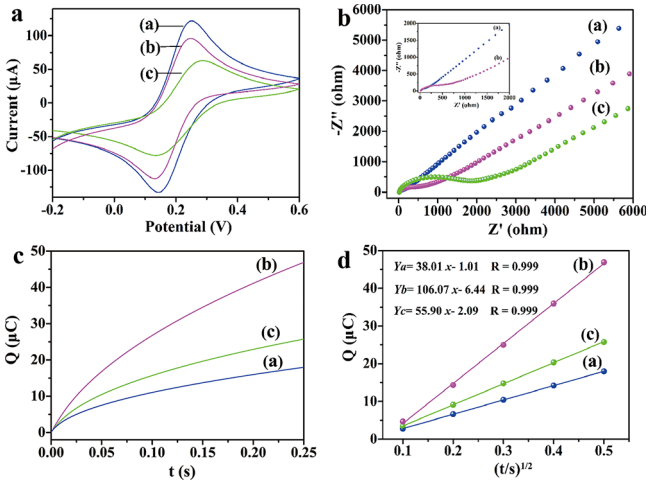

Figure 4. (a) CV curves; (b) Nyquist polts; (c) chronocoulometric curves, and (d) linear relationships between Q and $t^{1/2}$ of diverse working electrodes [(a) GCE, (b) β-Mo_2C/C/GCE, and (c) α-MoO_3/GCE].

that of α-MoO_3/GCE, ascribing to the good electrocatalytic activity of carbon-doping mesoporous β-Mo_2C. Therefore, compared with α-MoO_3, the CV test results indicate that β-Mo_2C/C has better electrical conductivity, thus effectively increasing the electron transport rate on the electrode surface. Generally, EIS technology is employed to analyze the interface charge and electron transfer behavior of electrochemical sensors. The Nyquist plot comprises of a semicircle in the high-frequency region and a straight line in the low-frequency region, indicating the occurrence of electron transfer and diffusion process at the electrode. Particularly, the semicircle diameter of the high-frequency region means the charge

https://dx.doi.org/10.1021/acsanm.0c01106
ACS Appl. Nano Mater. 2020, 3, 7499−7507

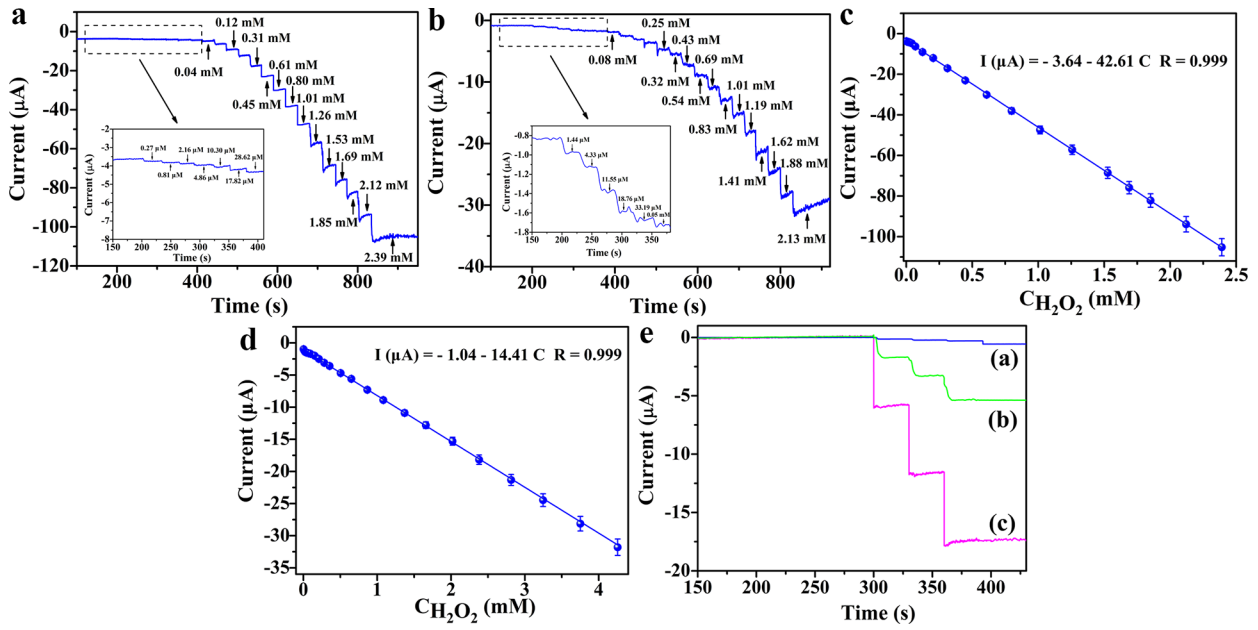

Figure 5. Typical *i-t* curves of β-Mo_2C/C/GCE (a) and α-MoO_3/GCE (b) with continuous injection of H_2O_2 (0.27 μM−2.39 mM) into 0.05 M PBS (pH = 7.4) at the applied potential of −0.4 V (inset: a partial magnified *i-t* curve in low H_2O_2 concentration range); corresponding calibration plots of β-Mo_2C/C/GCE (c) and α-MoO_3/GCE (d) for H_2O_2 sensing. Amperometric responses of different working electrodes (e) with continuous additions of 0.05 mM H_2O_2 into 0.05 M PBS (pH = 7.4) [(a) GCE, (b) α-MoO_3/GCE, and (c) β-Mo_2C/C/GCE)].

transfer resistance (R_{ct}). Thereby, it can be seen from Figure 4b that the β-Mo_2C/C and α-MoO_3 materials are successfully modified onto the bare GCE surface according to the semicircular changes of different modified electrodes. The β-Mo_2C/C/GCE has a tiny semicircular arc similar to bare GCE at the high-frequency region, indicating that the interface R_{ct} value is very small. In contrast, after modification with the α-MoO_3 material, a big semicircular diameter at the high-frequency region is observed, manifesting that the interface R_{ct} value of α-MoO_3/GCE is very large. The EIS test results are consistent with the CV data. Therefore, these results further reveal that β-Mo_2C/C has a better electrical conductivity than the α-MoO_3 material, which can accelerate the electron transfer on the electrode surface and enhance the electrocatalytic performance of trace H_2O_2.

The chronocoulometric curves of different modified electrodes were determined in 1.0 mM $K_3Fe(CN)_6$ solution containing 2.0 M KCl. Figure 4c clearly indicates that the relatively apparent surface area of diverse electrodes follows the sequence of β-Mo_2C/C/GCE > α-MoO_3/GCE > bare GCE. The effective surface area (A) of various working electrodes was estimated according to the following Anson's equation[39]

$$Q(t) = \frac{2nFAcD^{1/2}t^{1/2}}{\pi^{1/2}} + Q_{dl} + Q_{ads}$$

where n represents the charge transfer number; F is the Faraday constant; A characterizes effective electrode area; D is the diffusion coefficient in comparison of $[Fe(CN)_6]^{-3/-4}$ (7.6×10^{-6} $cm^2 \cdot s^{-1}$); Q_{dl} is the double-layer charge; Q_{ads} is the faradic charge; and t is the scanning time. According to the slope of the regression equation of Q-$t^{1/2}$ (Figure 4d), the corresponding A values for β-Mo_2C/C/GCE and α-MoO_3/GCE are 0.177 and 0.093 cm^2, respectively. These two values are very close to those calculated from the Randles-Sevcik equation (Supporting Information),[40−42] which gives the A value of 0.172 and 0.097 cm^2 for β-Mo_2C/C/GCE and α-MoO_3/GCE. The effective surface area of β-Mo_2C/C/GCE is ∼1.8−1.9 times greater than that of α-MoO_3/GCE. The large effective electrode area could increase the effective contact area with the electrolyte, providing more infiltrating space for the electrolyte to accelerate electron transfer, which is then helpful for the improvement of the electrochemical performance.[39] Therefore, the carbon-doping mesoporous β-Mo_2C material possesses not only good electronic conductivity but also well-electrocatalytic H_2O_2 performance.

Electrocatalytic Performance of Different Modified Electrodes toward H_2O_2. The chronoamperometry can be widely used to evaluate the electrocatalytic performance of the electrochemical sensor to H_2O_2. First, the operating potential, system pH value, and dripping volume on the electrode surface were explored. The optimal experimental conditions were defined as follows: (a) operating potential: −0.4 V, (b) solution pH value: 7.4, (c) dripping volume: 10 μL (Figure S8). With these optimal conditions at room temperature, the electrocatalytic properties of the β-Mo_2C/C/GCE and α-MoO_3/GCE electrodes toward H_2O_2 detection were investigated in 0.05 M phosphate-buffered solution (PBS) (pH = 7.4) accompanied by continuous stirring under N_2 flow. It should be indicated that the similar result can also be obtained under an air atmosphere except for the relatively large noise signal. With the addition of an H_2O_2 solution (0.27 μM−2.39 mM), the amperometric curves (*i-t* curves) with obvious stepwise enhancement for different modified electrodes were obtained (Figure 5a,b). It can be seen that both β-Mo_2C/C/GCE and α-MoO_3/GCE electrodes have good electrocatalytic performances toward H_2O_2 in a wide concentration range, and there are well-linear relationships in the curves of current response versus H_2O_2 concentration in the detection ranges of 0.27 μM−2.39 mM and 1.44 μM−2.13 mM, respectively (Figure 5c,d). The steady-state current of the β-Mo_2C/C/GCE response to H_2O_2 can reach a balance of 95% within 5 s. The sensitivity of 247.73 $\mu A\ mM^{-1}\ cm^{-2}$ for β-Mo_2C/C/GCE

https://dx.doi.org/10.1021/acsanm.0c01106
ACS Appl. Nano Mater. 2020, 3, 7499−7507

is larger than that of α-MoO_3/GCE (148.56 μA mM^{-1} cm^{-2}), while the estimated limit of detection (LOD) in the former (90 nM, S/N = 3) is 5 times that of the latter (480 nM, S/N = 3), and even far lower than the LOD of previously reported α-MoO_3/GO/GCE (310 nM, S/N = 3).[32] It should be pointed out that the estimated LOD has a little error in comparison with the calculated values (β-Mo_2C/C/GCE, 98 nM; α-MoO_3/GCE, 570 nM) according to IUPAC rule (Supporting Information).[43] Therefore, these results identify that the electrochemical sensor based on the β-Mo_2C/C/GCE electrode has a higher sensitivity, a lower detection limit, and a faster electrocatalytic response toward nanomolar-level H_2O_2.

The comparison of the electrocatalytic performance among the β-Mo_2C/C/GCE, α-MoO_3/GCE, and bare GCE electrodes to H_2O_2 is displayed in Figure 5e. With the continuous addition of 0.05 mM H_2O_2, the current response follows the order β-Mo_2C/C/GCE > α-MoO_3/GCE > bare GCE. The results show that the current response value of β-Mo_2C/C/GCE is 3.6 times greater than that of α-MoO_3/GCE. Furthermore, compared to the α-MoO_3 material, the electrochemical sensor based on β-Mo_2C/C also displays a lower detection limit, a wider linear detection region, and a faster electrocatalytic response toward H_2O_2. In addition, it can be seen from Table S4 that the electrocatalytic properties of the β-Mo_2C/C sensor to H_2O_2 are better than those of most reported metal oxides and metal oxides/carbon nanotubes (or *r*-GO) in recent years (references in Table S4). The higher sensitivity (247.73 μA mM^{-1} cm^{-2}) and lower detection limit (90 nM, S/N = 3) of β-Mo_2C/C/GCE toward H_2O_2 could be related to the good electronic conductivity and high catalytic activity that originated from the platinum-like structural Mo_2C[44,45] and carbon doping.[46] Therefore, compared with biological enzymes, precious metals, and their functionalized composites, the electrochemical sensor based on the β-Mo_2C/C sensing material has a good commercial application prospect in the detection of trace H_2O_2 owing to its outstanding advantages of low price, simple preparation, and friendly biocompatibility.

According to the above electrochemical experimental results and the reported literature,[47−49] the electrocatalytic mechanism of β-Mo_2C/C/GCE to H_2O_2 can be described as follows

$$H_2O_2 + e^- \rightarrow OH_{ad} + OH^- \quad (a)$$

$$OH_{ad} + e^- \rightarrow OH^- \quad (b)$$

$$2OH^- + 2H^+ \rightarrow 2H_2O \quad (c)$$

In the electrocatalytic reaction, H_2O_2 first captures one electron to form the unstable intermediate OH_{ad} (eq a), which can easily obtain another electron to generate a stable OH^- (eq b). Therefore, the generation of unstable intermediate OH_{ad} is the key control step in H_2O_2 electrocatalytic redox reaction. The inherent characteristics of mesoporous β-Mo_2C/C hierarchical structure play important roles in its electrocatalysis of H_2O_2, which can be explained as follows: (i) the mesoporous structure is beneficial to shorten the diffusion path and accelerate the charge transfer at the electrode−electrolyte interface,[25,50] further improving electron transfer rate and mass transfer efficiency; (ii) the large effective surface area (*A*) supply more active sites on the electrode surface and facilitate the diffusion of analytes, which provides a highly efficient platform for electrochemical detection of H_2O_2; (iii) the synergistic effects of platinum-like electron structural Mo_2C and doped carbon can effectively improve the catalytic activity and the electronic conductivity of the electrochemical sensor constructed from β-Mo_2C/C and rapidly promote the H_2O_2 electrocatalytic reaction on the electrode surface. Therefore, all these factors result in the excellent sensing performance of this electrochemical sensor in the detection of nanomolar-level H_2O_2.

Selectivity, Stability, Reproducibility, and Practicability of the β-Mo_2C/C/GCE Sensor. As is known to all, the poor selectivity can lead to the false result, and thus the selectivity of the electrochemical sensor is one of the most important factors for evaluating its application in practice. To explore the selectivity of the β-Mo_2C/C/GCE sensor toward H_2O_2, 0.05 mM H_2O_2 together with 0.5 mM common interfering species, for instance, $NaNO_2$, glucose (Glu), ascorbic acid (AA), uric acid (UA), threonine (Thr), and cysteine (Cys),[51,52] were continuously added into the PBS (0.05 M, pH = 7.4) solution during the electrocatalytic measurements. As shown in Figure S9a, it can be seen that no additional amperometric response is observed after the addition of the above interfering species, despite their 10 times concentrations rather than H_2O_2. Furthermore, the steplike amperometric current is sharply enhanced after the addition of H_2O_2, and the current response quickly returns to a stable state within 5 s in the presence of interfering substances. The results indicate that the determination of H_2O_2 is not influenced under the existence of the above-mentioned interfering species. This is mainly ascribed to the following points: (i) the H_2O_2 has a good reaction activity on the basis of the cleavage of the O−O bond;[51] (ii) at the optimal potential of −0.4 V, no obvious electrical signal was detected for these interfering reagents, indicating that these substances were hardly to be reduced at −0.4 V. Therefore, the β-Mo_2C/C/GCE sensor toward H_2O_2 has good selectivity and strong anti-interference ability to the common interfering substances.

Also, the stability and reproducibility of the electrochemical sensor are two important indexes to evaluate the performance toward H_2O_2 in a practical application. The β-Mo_2C/C/GCE sensor was placed in an environment of 4 °C and measured every 6 d by adding 0.05 mM H_2O_2 into the PBS solution. The current response can maintain 90% of the initial sensitivity with the relative standard deviation (RSD) being lower than 2.68% (Figure S9b), indicating the good stability of the electrochemical sensor for H_2O_2 detection. To determine the reproducibility, the five separate β-Mo_2C/C/GCE sensors fabricated simultaneously were measured according to the above method. The result in Figure S9c shows that the RSD is less than 2.5%. Furthermore, the same electrode was continuously tested five times in the PBS solution containing 0.05 mM H_2O_2 (Figure S9d), and the RSD of the current response is ∼2.1%. These results demonstrate that the β-Mo_2C/C/GCE electrode prepared by a simple drop-coating method has satisfactory reproducibility for H_2O_2 detection.

To assess the practicability of the nonenzymatic H_2O_2 sensor in a real application, the electrochemical sensor based on β-Mo_2C/C/GCE was applied to the detection of H_2O_2 in real human serum specimens. In view of the fact that the high viscosity of human serum after a centrifugal treatment can affect the accuracy of the test, the above specimens were centrifuged and diluted 40 times with PBS (0.05 M, pH = 7.4) before the measurement. Subsequently, the recovery of different concentrations of H_2O_2 spiked into the human serum specimens was determined by a standard addition

https://dx.doi.org/10.1021/acsanm.0c01106
ACS Appl. Nano Mater. 2020, 3, 7499−7507

method.[52,53] The results in Table 1 show that the average recovery is in the range of 96.4−100.5% and that the RSD varies from 1.03−2.26%, illustrating that the test method has satisfactory accuracy and that the results exhibit good practicality for the electrochemical detection of H_2O_2 in real human serum specimens. Therefore, it can be expected that the nonenzymatic β-Mo_2C/C/GCE electrochemical sensor with higher sensitivity and lower detection limit could be used in real-time to detect nanomolar-level H_2O_2 in the fields of disease diagnosis, biological analysis, environmental production, and food safety.

Table 1. Determination of H_2O_2 in Real Human Serum Specimens using β-Mo_2C/C/GCE Electrochemical Sensor

human serum specimens	H_2O_2 added (μM)	H_2O_2 found (μM)	recovery (%)	RSD (%)
1	20	19.28	96.4	1.11
2	40	40.19	100.5	2.26
3	60	59.71	99.5	1.03

CONCLUSIONS

In summary, carbon-doping mesoporous β-Mo_2C and α-MoO_3 hierarchical structures constructed from nanoparticles were simply prepared by a one-step calcination of the single-crystal $[(H_2L)_2(Mo_8O_{26})]_n$ precursor in N_2/H_2 and air atmospheres, respectively. The β-Mo_2C/C/GCE sensor fabricated by a simple drop-coating method was efficiently used to detect H_2O_2 in real human serum specimens for the first time. Compared with the α-MoO_3/GCE electrode and most reported metal oxides sensing materials, the β-Mo_2C/C/GCE sensor displays good nanomolar electrochemical detection of H_2O_2, which originated from the synergistic effect of inherent characteristics of β-Mo_2C/C material involving the hierarchical nanostructure, uniform mesopore, large surface area, platinum-like electronic structural β-Mo_2C, and carbon doping. This work not only provides a simple synthesis strategy of mesoporous metal carbide hierarchical nanostructure but also sets up a new route for developing efficient nonenzymatic electrochemical sensors. Furthermore, its satisfactory determination of H_2O_2 in real human serum specimens provides the possibility for its practical application.

ASSOCIATED CONTENT

Supporting Information

The Supporting Information is available free of charge at https://pubs.acs.org/doi/10.1021/acsanm.0c01106.

Chemical reagents, characterization instruments, synthesis of single crystal, crystallography details including data and structure refinement, selected bond lengths and angles, modified electrodes (fabrication and measurements), peak assignments of IR spectrum, TG curves, XPS spectra, SEM images, optimization of experimental conditions, plots of current versus time and current versus volume, comparison of electrodes, additional references (PDF)

AUTHOR INFORMATION

Corresponding Authors

Zhao-Peng Deng − *Key Laboratory of Functional Inorganic Material Chemistry, Ministry of Education, School of Chemistry and Materials Science, Heilongjiang University, Harbin 150080, People's Republic of China*; Email: dengzhaopeng@hlju.edu.cn

Shan Gao − *Key Laboratory of Functional Inorganic Material Chemistry, Ministry of Education, School of Chemistry and Materials Science, Heilongjiang University, Harbin 150080, People's Republic of China*; orcid.org/0000-0001-6370-4994; Email: shangao67@yahoo.com

Authors

Bo Li − *Key Laboratory of Functional Inorganic Material Chemistry, Ministry of Education, School of Chemistry and Materials Science, Heilongjiang University, Harbin 150080, People's Republic of China; College of Science, Heihe University, Heihe 164300, People's Republic of China*

Li-Hong Liu − *Key Laboratory of Functional Inorganic Material Chemistry, Ministry of Education, School of Chemistry and Materials Science, Heilongjiang University, Harbin 150080, People's Republic of China; College of Science, Heihe University, Heihe 164300, People's Republic of China*

Hai-Yan Song − *Key Laboratory of Functional Inorganic Material Chemistry, Ministry of Education, School of Chemistry and Materials Science, Heilongjiang University, Harbin 150080, People's Republic of China*

Li-Hua Huo − *Key Laboratory of Functional Inorganic Material Chemistry, Ministry of Education, School of Chemistry and Materials Science, Heilongjiang University, Harbin 150080, People's Republic of China*; orcid.org/0000-0003-1725-0148

Complete contact information is available at: https://pubs.acs.org/10.1021/acsanm.0c01106

Notes

The authors declare no competing financial interest.

ACKNOWLEDGMENTS

This work is financially supported by the National Natural Science Foundation of China (51302067), the Interational Science & Technology Cooperation Program of China (2016YFE0115100), the Scientific and Technological Innovation Talents of Harbin (2016RAQXJ005), the Young Innovation Talents of college in Heilongjiang Province (UNPYSCT-2016074), the Basic Research Business Fees of Colleges and Universities in Heilongjiang Province (Grant No. 2018-KYYWF-1266), the Basic Research Business Fees of Colleges and Universities in Heilongjiang Province (Grant No. 2019-KYYWF-0456), and the Heilongjiang University Ph.D. Innovation Research Project (YJSCX2019-021HLJU).

REFERENCES

(1) Sarhan, R. M.; El-Nagar, G. A.; Abouserie, A.; Roth, C. Silver-Iron Hierarchical Microflowers for Highly Efficient H_2O_2 Nonenzymatic Amperometric Detection. *ACS Sustainable Chem. Eng.* **2019**, *7*, 4335−4342.

(2) Waldiya, M.; Bhagat, D.; R, N.; Singh, S.; Kumar, A.; Ray, A.; Mukhopadhyay, I. Development of highly sensitive H_2O_2 redox sensor from electrodeposited tellurium nanoparticles using ionic liquid. *Biosens. Bioelectron.* **2019**, *132*, 319−325.

(3) Zhang, R. Z.; Chen, W. Recent advances in graphene-based nanomaterials for fabricating electrochemical hydrogen peroxide sensors. *Biosens. Bioelectron.* **2017**, *89*, 247−268.

(4) Asif, M.; Liu, H. W.; Aziz, A.; Wang, H. T.; Wang, Z. Y.; Ajmal, M.; Xiao, F.; Liu, H. F. Core-shell iron oxide-layered double hydroxide: High electrochemical sensing performance of H_2O_2

biomarker in live cancer cells with plasma therapeutics. *Biosens. Bioelectron.* **2017**, *97*, 352−359.
(5) Asif, M.; Aziz, A.; Azeem, M.; Wang, Z. Y.; Ashraf, G.; Xiao, F.; Chen, X. D.; Liu, H. F. A review on electrochemical biosensing platform based on layered double hydroxides for small molecule biomarkers determination. *Adv. Colloid Interface Sci.* **2018**, *262*, 21−38.
(6) Asif, M.; Wang, H. T.; Dong, S.; Aziz, A.; Zhang, G. A.; Xiao, F.; Liu, H. F. Metal oxide intercalated layered double hydroxide nanosphere: With enhanced electrocatalyic activity towards H_2O_2 for biological applications. *Sens. Actuators, B* **2017**, *239*, 243−252.
(7) Ren, M.; Deng, B.; Wang, J. Y.; Kong, X.; Liu, Z. R.; Zhou, K.; He, L.; Lin, W. A Fast Responsive Two-Photon Fluorescent Probe for Imaging H_2O_2 in Lysosomes with a Large Turn-On Fluorescence Signal. *Biosens. Bioelectron.* **2016**, *79*, 237−243.
(8) Li, D.; Wang, M.; Cheng, N.; Xue, X.; Wu, L.; Cao, W. A Modified FOX-1 Method for Micro-Determination of Hydrogen Peroxide in Honey Samples. *Food Chem.* **2017**, *237*, 225−231.
(9) Bai, W. S.; Zhang, X. J.; Zheng, J. B. Direct Growth of Ordered Pd Cu and Co Doped Pd Cu Nanoparticles on Graphene Oxide Based on a One-Step Hydrothermal Method for Ultrasensitive Sensing of H_2O_2 in Living Cells. *Analyst* **2019**, *144*, 157−160.
(10) Liu, M.-M.; Li, S.-H.; Huang, D.-D.; Xu, Z.-W.; Wu, Y.-W.; Lei, Y.; Liu, A.-L. MoO_x quantum dots with peroxidase-like activity on microfluidic paperbased analytical device for rapid colorimetric detection of H_2O_2 released from PC12 cells. *Sens. Actuators, B* **2020**, *305*, 127512.
(11) Dai, H. X.; Chen, Y. L.; Niu, X. Y.; Pan, C. J.; Chen, H. L.; Chen, X. G. High-Performance Electrochemical Biosensor for Nonenzymatic H_2O_2 Sensing Based on Au@C-Co_3O_4 Heterostructures. *Biosens. Bioelectron.* **2018**, *118*, 36−43.
(12) Shu, Y.; Xu, J.; Chen, J.; Xu, Q.; Xiao, X.; Jin, D.; Pang, H.; Hu, X. Ultrasensitive Electrochemical Detection of H_2O_2 In Living Cells Based on Ultrathin MnO_2 Nanosheets. *Sens. Actuators, B* **2017**, *252*, 72−78.
(13) Han, L.; Yang, D. P.; Liu, A. H. Leaf-Templated Synthesis of 3D Hierarchical Porous Cobalt Oxide Nanostructure as Direct Electrochemical Biosensing Interface with Enhanced Electrocatalysis. *Biosens. Bioelectron.* **2015**, *63*, 145−152.
(14) Chakraborty, P.; Dhar, S.; Debnath, K.; Mondal, S. P. Glucose and Hydrogen Peroxide Dual-Mode Electrochemical Sensing Using Hydrothermally Grown CuO Nanorods. *J. Electroanal. Chem.* **2019**, *833*, 213−220.
(15) Yang, K.; Zhong, H.; Cheng, Z. P.; Li, X. R.; Zhang, A. R.; Li, T. L.; Zhang, Y. J.; Liu, G. Q.; Qian, H. Y. Magnetic Fe_3O_4 Stacked Sphere-Like Nanocomposite and Its Application as Platform for H_2O_2 Sensing. *J. Electroanal. Chem.* **2018**, *814*, 1−6.
(16) Balasubramanian, P.; Annalakshmi, M.; Chen, S.-M.; Sathesh, T.; Peng, T.-K.; Balamurugan, T. S. T. Facile Solvothermal Preparation of Mn_2CuO_4 Microspheres: Excellent Electrocatalyst for Real-Time Detection of H_2O_2 Released from Live Cells. *ACS Appl. Mater. Interfaces* **2018**, *10*, 43543−43551.
(17) Bracamonte, M. V.; Melchionna, M.; Giuliani, A.; Nasi, L.; Tavagnacco, C.; Prato, M.; Fornasiero, P. H_2O_2 Sensing Enhancement by Mutual Integration of Single Walled Carbon Nanohorns with Metal Oxide Catalysts: The CeO_2 Case. *Sens. Actuators, B* **2017**, *239*, 923−932.
(18) Chirizzi, D.; Guascito, M. R.; Filippo, E.; Malitesta, C.; Tepore, A. A novel Nonenzymatic Amperometric Hydrogen Peroxide Sensor Based on CuO@Cu_2O Nanowires Embedded into Poly(vinyl alcohol). *Talanta* **2016**, *147*, 124−131.
(19) Asif, M.; Aziz, A.; Wang, Z. Y.; Ashraf, G.; Wang, J. L.; Luo, H. B.; Chen, X. D.; Xiao, F.; Liu, H. F. Hierarchical CNTs@CuMn Layered Double Hydroxide Nanohybrid with Enhanced Electrochemical Performance in H_2S Detection from Live Cells. *Anal. Chem.* **2019**, *91*, 3912−3920.
(20) Zeng, X. Q.; Gao, X. H.; Li, G. R.; Sun, M. H.; Lin, Z.; Ling, M.; Zheng, J. C.; Liang, C. D. Conductive Molybdenum Carbide as The Polysulfide Reservoir for Lithium-Sulfur Batteries. *J. Mater. Chem. A* **2018**, *6*, 17142−17147.
(21) Dong, J.; Wu, Q.; Huang, C. P.; Yao, W. F.; Xu, Q. N. Cost Effective Mo Rich Mo_2C Electrocatalysts for the Hydrogen Evolution Reaction. *J. Mater. Chem. A* **2018**, *6*, 10028−10035.
(22) Zhai, Q. F.; Zhang, X. W.; Li, J.; Wang, E. K. Molybdenum Carbide Nanotubes: a Novel Multifunctional Material for Label-Free Electrochemical Immunosensing. *Nanoscale* **2016**, *8*, 15303−15308.
(23) Huang, Q.; Li, X. K.; Feng, S. X.; Zhuge, W. F.; Liu, F. P.; Peng, J. Y.; Mo, S. C. An electrochemical Sensor Based on the Composite of Molybdenum Carbides and a Multiwalled Carbon Nanotube Modified Electrode for the Ultrasensitive Detection of Rifampicin. *Anal. Methods* **2018**, *10*, 3594−3601.
(24) Tian, L.; Qi, J. X.; Ma, X. Y.; Wang, X. J.; Yao, C.; Song, W.; Wang, Y. H. A Facile DNA Strand Displacement Reaction Sensing Strategy of Electrochemical Biosensor Based on N-Carboxymethyl Chitosan/Molybdenum Carbide Nanocomposite for Micro RNA-21 Detection. *Biosens. Bioelectron.* **2018**, *122*, 43−50.
(25) Zhang, L.; Zhang, J. Multiporous Molybdenum Carbide Nanosphere as a New Charming Electrode Material for Highly Sensitive Simultaneous Detection of Guanine and Adenine. *Biosens. Bioelectron.* **2018**, *110*, 218−224.
(26) Ren, H. L.; Zhang, Y.; Liu, L. L.; Li, Y. G.; Wang, D. Y.; Zhang, R. Y.; Zhang, W. J.; Li, Y. C.; Ye, B. C. Synthesis of hollow Mo_2C/carbon spheres, and their application to simultaneous electrochemical detection of hydroquinone, catechol, and resorcinol. *Microchim. Acta* **2019**, *186*, 306−314.
(27) Fan, M. H.; Chen, H.; Wu, Y. Y.; Feng, L. L.; Liu, Y. P.; Li, G. D.; Zou, X. X. Growth of Molybdenum Carbide Micro-Islands on Carbon Cloth Toward Binder-Free Cathodes for Efficient Hydrogen Evolution Reaction. *J. Mater. Chem. A* **2015**, *3*, 16320−16326.
(28) Xiao, P.; Yan, Y.; Ge, X. M.; Liu, Z. L.; Wang, J. Y.; Wang, X. Investigation of Molybdenum Carbide Nano-Rod as an Efficient and Durable Electrocatalyst for Hydrogen Evolution in Acidic and Alkalilne Media. *Appl. Catal., B* **2014**, *154*, 232−237.
(29) Seh, Z. W.; Fredrickson, K. D.; Anasori, B.; Kibsgaard, J.; Strickler, A. L.; Lukatskaya, M. R.; Gogotsi, Y.; Jaramillo, T. F.; Vojvodic, A. Two-Dimensional Molybdrnum Carbide (MXene) as an Efficient Electrocatalyst for Hydrogen Evolution. *ACS Energy Lett.* **2016**, *1*, 589−594.
(30) Wu, H. B.; Xia, B. Y.; Yu, L.; Yu, X. Y.; Lou, X. W. Porous Molybdenum Carbide Nano-Octahedrons Synthesized via Confined Carburization in Metal-Organic Frameworks for Efficient Hydrogen Production. *Nat. Commun.* **2015**, *6*, 6512−6519.
(31) Yu, F. Y.; Gao, Y.; Lang, Z. L.; Ma, Y. Y.; Yin, L. Y.; Du, J.; Tan, H. Q.; Wang, Y. H.; Li, Y. G. Electrocatalytic Performance of Ultrasmall Mo_2C Affected by Different Transition Metal Dopants in Hydrogen Evolution Reaction. *Nanoscale* **2018**, *10*, 6080−6087.
(32) Li, B.; Song, H. Y.; Deng, Z. P.; Huo, L. H.; Gao, S. Novel sensitive amperometric hydrogen peroxide sensor using layered hierarchical porous α-MoO_3 and GO modified glass carbon electrode. *Sens. Actuators, B* **2019**, *288*, 641−648.
(33) Gao, Q.; Zhao, X. Y.; Xiao, Y.; Zhao, D.; Cao, M. H. A mild route to mesoporous Mo_2C−C hybrid nanospheres for high performance lithium-ion batteries. *Nanoscale* **2014**, *6*, 6151−6157.
(34) Liu, X. X.; Zhang, L.; Lan, X. W.; Hu, X. L. Paragenesis of Mo_2C nanocrystals in mesoporous carbon nanofibers for electrocatalytic hydrogen evolution. *Electrochim. Acta* **2018**, *274*, 23−30.
(35) Luo, Y.; Jin, C.; Wang, Z. J.; Wei, M. H.; Yang, C. H.; Yang, R. Z.; Chen, Y.; Liu, M. L. A high-performance oxygen electrode for Li-O_2 batteries: Mo_2C nanoparticles grown on carbon fibers. *J. Mater. Chem. A* **2017**, *5*, 5690−5695.
(36) Humagain, G.; MacDougal, K.; MacInnis, J.; Lowe, J. M.; Coridan, R. H.; MacQuarrie, S.; Dasog, M. Highly Effcient, Biochar-Derived Molybdenum Carbide Hydrogen Evolution Electrocatalyst. *Adv. Energy Mater.* **2018**, *8*, 1801461−1801465.
(37) Lin, H. L.; Shi, Z. P.; He, S.; Yu, X.; Wang, S.; Gao, Q. S.; Tang, Y. Heteronanowires of MoC-Mo_2C as Efficient Electrocatalysts for Hydrogen Evolution Reaction. *Chem. Sci.* **2016**, *7*, 3399−3405.

https://dx.doi.org/10.1021/acsanm.0c01106
ACS Appl. Nano Mater. 2020, 3, 7499−7507

(38) Liu, Y. C.; Huang, B. B.; Xie, Z. L. Hydrothermal Synthesis of Core-Shell MoO_2/α-Mo_2C Heterojunction as High Performance Electrocatalyst for Hydrogen Evolution Reaction. *Appl. Surf. Sci.* **2018**, *427*, 693−701.
(39) Dong, Y. Y.; Zhang, L. Constructed 3D Hierarchical Porous Wool-Ball-Like NiO-Loaded AlOOH Electrode Materials for the Determination of Toxic Metal Ions. *Electrochim. Acta* **2018**, *271*, 27−34.
(40) Aziz, A.; Asif, M.; Azeem, M.; Ashraf, G.; Wang, Z. Y.; Xiao, F.; Liu, H. F. Self-stacking of exfoliated charged nanosheets of LDHs and graphene as biosensor with real-time tracking of dopamine from live cells. *Anal. Chim. Acta* **2019**, *1047*, 197−207.
(41) Asif, M.; Aziz, A.; Ashraf, G.; Wang, Z. Y.; Wang, J. L.; Azeem, M.; Chen, X. D.; Xiao, F.; Liu, H. F. Facet-Inspired Core-Shell Gold Nanoislands on Metal Oxide Octadecahedral Heterostructures: High Sensing Performance toward Sulfide in Biotic Fluids. *ACS Appl. Mater. Interfaces* **2018**, *10*, 36675−36685.
(42) Asif, M.; Aziz, A.; Wang, H. T.; Wang, Z. Y.; Wang, W.; Ajmal, M.; Xiao, F.; Chen, X. D.; Liu, H. F. Superlattice stacking by hybridizing layered double hydroxide nanosheets with layers of reduced graphene oxide for electrochemical simultaneous determination of dopamine, uric acid and ascorbic acid. *Microchim. Acta* **2019**, *186*, 61.
(43) Asif, M.; Wang, H. T.; Shuang, D.; Aziz, A.; Zhang, G. A.; Xiao, F.; Liu, H. F. Metal oxide intercalated layered double hydroxide nanosphere: With enhanced electrocatalyic activity towards H_2O_2 for biological applications. *Sens. Actuators, B* **2017**, *239*, 243−252.
(44) Ouyang, T.; Ye, Y.-Q.; Wu, C.-Y.; Xiao, K.; Liu, Z.-Q. Heterostructures Composed of N-Doped Carbon Nanotubes Encapsulating Cobalt and β-Mo_2C Nanoparticles as Bifunctional Electrodes for Water Splitting. *Angew. Chem., Int. Ed.* **2019**, *58*, 4923−4928.
(45) Li, M. X.; Zhu, Y.; Wang, H. Y.; Wang, C.; Pinna, N.; Lu, X. F. Ni Strongly Coupled with Mo_2C Encapsulated in Nitrogen-Doped Carbon Nanofibers as Robust Bifunctional Catalyst for Overall Water Splitting. *Adv. Energy Mater.* **2019**, *9*, 1803185−1803195.
(46) Wang, Z.; Xu, X.; Liu, Z.; Ji, S.; Ahmed Idris, S. O.; Liu, J. Hollow spheres of Mo_2C@C as synergistically confining sulfur host for superior Li-S battery cathode. *Electrochim. Acta* **2020**, *332*, 135482−135491.
(47) Wang, Y. G.; Wang, Y. L.; Wu, D.; Ma, H. M.; Zhang, Y.; Fan, D. W.; Pang, X. H.; Du, B.; Wei, Q. Label-Free Electrochemical Immunosensor Based on Flower-Like Ag/MoS_2/rGO Nanocomposites for Ultrasensitive Detection of Carcinoembryonic Antigen. *Sens. Actuators, B* **2018**, *255*, 125−132.
(48) Zhu, D.; Zuo, J. W.; Tan, L. C.; Pang, H. J.; Ma, H. Y. Enzymeless Electrochemical Determination of Hydrogen Peroxide at a Heteropolyanion-Based Composite Film Electrode. *New J. Chem.* **2019**, *43*, 1053−1062.
(49) Alexander, M.; Suriyadharshini, S.; Raghu, S.; Kalaivani, R. A.; Gnanam, S. Semiconducting material of pure ZnO hollow nanospheres; and their modified electrode used for electrocatalytic reduction of ethanol and hydrogen peroxide. *Mater. Sci. Semicond. Process.* **2019**, *99*, 62−67.
(50) Vu, A.; Qian, Y. Q.; Stein, A. Porous Electrode Materials for Lithium-Ion Batteries-How to Prepare Them and What Makes Them Special. *Adv. Energy Mater.* **2012**, *2*, 1056−1085.
(51) Shu, Y. J.; Zhang, L. L.; Cai, H. H.; Yang, Y.; Zeng, J. C.; Ma, D.; Gao, Q. S. Hierarchical Mo_2C@MoS_2 nanorods as electrochemical sensors for highly sensitive detection of hydrogen peroxide and cancer cells. *Sens. Actuators, B* **2020**, *311*, 127863−127873.
(52) Song, H. Y.; Zhao, H.; Zhang, X. F.; Xu, Y. M.; Cheng, X. L.; Gao, S.; Huo, L. H. A hollow urchin-like α-MnO_2 as an electrochemical sensor for hydrogen peroxide and dopamine with high selectivity and sensitivity. *Microchim. Acta* **2019**, *186*, 210−221.
(53) Gao, J.; Liu, H.; Tong, C.; Pang, L.; Feng, Y.; Zuo, M.; Wei, Z.; Li, J. Hemoglobin-$Mn_3(PO_4)_2$ hybrid nanoflower with opulent electroactive centers for high-performance hydrogen peroxide electrochemical biosensor. *Sens. Actuators, B* **2020**, *307*, 127628−127637.

https://dx.doi.org/10.1021/acsanm.0c01106
ACS Appl. Nano Mater. 2020, 3, 7499−7507